Mon. Not. R. Astron. Soc. **368,** 1301–1310 (2006) doi:10.1111/j.1365-2966.2006.10222.x

On the population of primordial star clusters in the presence of ultraviolet background radiation

Michael A. MacIntyre,[1⋆] Fernando Santoro[2] and Peter A. Thomas[1]

[1]*Astronomy Centre, University of Sussex, Falmer, Brighton BN1 9QH*
[2]*Centre for Astrophysics and Space Astronomy, University of Colorado, 389 UCB, Boulder, CO 80309-0389, USA*

Accepted 2006 February 13. Received 2006 February 13; in original form 2005 October 4

ABSTRACT

We use the algorithm of Cole et al. to generate merger trees for the first star clusters in a Λ cold dark matter (ΛCDM) cosmology under an isotropic ultraviolet background radiation field, parametrized by J_{21}. We have investigated the problem in two ways: a global radiation background and local radiative feedback surrounding the first star clusters.

Cooling in the first haloes at high redshift is dominated by molecular hydrogen, H_2 – we call these Generation 1 objects. At lower redshift and higher virial temperature, $T_{\rm vir} \gtrsim 10^4$ K, electron cooling dominates – we call these Generation 2.

Radiation fields act to photodissociate H_2, but also generate free electrons that can help to catalyze its production. At modest radiation levels, $J_{21}/(1+z)^3 \sim 10^{-12}$–$10^{-7}$, the nett effect is to enhance the formation of Generation 1 star clusters. At higher fluxes, the heating from photoionization dominates and halts their production. With a realistic build-up of flux over time, the period of enhanced H_2 cooling is so fleeting as to be barely discernable and the nett effect is to move primordial star cluster formation towards Generation 2 objects at lower redshift.

A similar effect is seen with local feedback. Provided that enough photons are produced to maintain ionization of their host halo, they will suppress the cooling in Generation 1 haloes and boost the numbers of primordial star clusters in Generation 2 haloes. Significant suppression of Generation 1 haloes occurs for specific photon fluxes in excess of about 10^{43} ph s^{-1} M$_\odot^{-1}$.

Key words: galaxies: formation – galaxies: star clusters.

1 INTRODUCTION

Primordial star clusters contain the first stars to form in the Universe, from zero-metallicity gas. Previous work (e.g. Tegmark et al. 1997; Abel et al. 1998; Bromm, Coppi & Larson 1999; Hutchings et al. 2002; Santoro & Thomas 2003) has concentrated on the very first objects for which there is no significant external radiation field. However, these first clusters are expected to produce massive stars which will irradiate the surrounding Universe and may well be responsible for partial re-ionization of the intergalactic medium (IGM).

The only species produced in sufficient abundance to affect the cooling at early times is molecular hydrogen. Its presence allows the first objects to cool and form in low-temperature haloes ($T < 10^4$ K) at high redshift ($z_{\rm vir} \sim 20$–30). However, molecular hydrogen is very fragile and can easily be dissociated by ultraviolet (UV) photons in the Lyman–Werner bands, (11.2–13.6 eV). Thus, the formation of the first stars may well have a negative feedback effect on subsequent Population III star formation by suppressing cooling via this mechanism. This problem is not a trivial one and has been the subject of much interest in recent years (e.g. Haiman, Rees & Loeb 1996; Haiman, Abel & Rees 2000; Kitayama et al. 2000; Glover & Brand 2001; Machacek, Bryan & Abel 2001; Omukai 2001; Oh & Haiman 2002; Ricotti, Gnedin & Shull 2002; Cen 2003; Ciardi, Ferrara & White 2003; Yoshida et al. 2003; Tumlinson, Venkatesan & Shull 2004). The complexity of the feedback and the large number of unknowns [e.g. Population III initial mass function (IMF), total ionizing photon production, etc.] make this problem very challenging.

In an attempt to understand this era of primordial star cluster formation, we investigated in a previous paper (Santoro & Thomas 2003, hereafter ST03) the merger history of primordial haloes in the Λ cold dark matter (ΛCDM) cosmology. There we assumed no external radiation field [other than that provided by cosmic microwave background (CMB) photons]. The Block Model of Cole &

⋆E-mail: m.a.macintyre@sussex.ac.uk

Kaiser (1988) was used to generate the merger history of star clusters, using a simple model for the collapse and cooling criterion, hence identifying those haloes that were able to form stars before being disrupted by mergers. We then contrasted the mass functions of all the resulting star clusters and those of primordial composition, that is, star clusters that have not been contaminated by subclusters inside them. We found two generations of primordial haloes: low-temperature clusters that cool via H_2, and high-temperature clusters that cool via electronic transitions.

We investigated two regions of space each enclosing a mass of $10^{11}\,h^{-1}\,M_\odot$: a high-density region corresponding to a 3σ fluctuation ($\delta_0 = 10.98$), and a mean-density region ($\delta_0 = 0$), where δ_0 is the initial overdensity of the root block. In the high-density region, we found that approximately half of the star clusters are primordial. The fractional mass contained in the two generations was 0.109 in low-temperature clusters and 0.049 in high-temperature clusters. About 16 per cent of all baryons in this region of space were once part of a primordial star cluster. In the low-density case, the fractional mass in the two generations was almost unchanged, but the haloes collapsed at much lower redshifts and the mass function was shifted towards higher masses.

In this paper, as a continuation of the previous work, we include the effect of ionizing radiation in two different ways: first, we add a homogeneous background radiation field; secondly, we consider feedback from the first star clusters formed in the merger tree – these will form an ionizing (and photodissociating) sphere around them, changing the cooling properties of neighbouring star clusters. A further improvement upon our previous work includes the use of a more realistic merger tree.

We describe our chemical network including radiative processes in Section 2, and the new merger tree method in Section 3. The effect of a global ionization field on the formation of stars in primordial star clusters is considered in Section 4 and that of local feedback in Section 5. Finally, we summarize our conclusions in Section 6.

2 PRIMORDIAL CHEMISTRY AND GAS COOLING IN THE PRESENCE OF RADIATION

2.1 Chemical model

In this section, we introduce the chemical network needed to follow the coupled chemical and thermal evolution under a homogeneous UV background radiation field.

The non-equilibrium chemistry code is based on the minimal model presented in Hutchings et al. (2002, hereafter HSTC02). It calculates the evolution of the following nine species: H_2, H, H^+, H_2^+, H^-, He, He^+, He^{++} and e^-. The important cooling processes are: molecular hydrogen cooling, collisional excitation and ionization of atomic hydrogen, collisional excitation of He^+, and inverse Compton cooling from CMB photons. In this paper, we only consider the low density–high temperature ($T > 300\,K$) limit. Thus, we have ignored the effects of HD cooling, which is only important in the high density–low temperature regime.

To this chemical model, we have added the photoionization and photodissociation reactions compiled by Abel et al. (1997) and listed in Table 1 with rates determined as in Appendix A. This consists of nine reactions involving the interaction of each species with the background photons. These are: photoionization of H, He, He^+ and H_2, with threshold energies of $h\nu = 13.6$, 24.6, 54.4 and 15.42 eV, respectively; photodetachment of H^- with a threshold energy of 0.755 eV, potentially an important process since H^- catalyzes the formation of H_2; and photodissociation of H_2^+ and H_2 (by the Solomon process and by direct photodissociation). In the case of the Solomon process, dissociation happens in a very narrow energy range $12.24 < h\nu < 13.51$ eV.

The energy equation takes the following form:

$$\frac{\mathrm{d}(n_\mathrm{t}T)}{\mathrm{d}t} = \frac{2}{3k}\left(\Lambda_\mathrm{heat} - \Lambda_\mathrm{cool}\right), \qquad (1)$$

where n_t is the total number density of all species, T is the temperature, Λ_cool and Λ_heat are the cooling and heating terms,

Table 1. This table summarizes the important reactions that should be included in a chemical network if a uniform background radiation field is present. Compiled by Abel et al. (1997), except cross-sections 25 and 27. The number index of each reaction corresponds to those in that paper. Reference: Osterbrock (1989, O89), de Jong (1972, DeJ72), O'Neil & Reinhardt (1978, OR78), Tegmark et al. (1997, TSR97), Haiman et al. (1996, HRL96) and Abel et al. (1997, AAZN97).

	Reaction	Cross-sections (cm^{-2})	Reference
20	$H + \gamma \longmapsto H^+ + 2e^-$	$\sigma_{20} = A_0\left(\frac{\nu}{\nu_\mathrm{th}}\right)^{-4}\left[\frac{e^{(4-4\arctan\epsilon/\epsilon)}}{(1-e^{-2\pi/\epsilon})}\right]$ $\begin{cases} A_0 = 6.30\times10^{-18}\,\mathrm{cm}^2 \\ \epsilon = \sqrt{\nu/\nu_\mathrm{th}-1}, \quad h\nu_\mathrm{th} = 13.6\,\mathrm{eV} \end{cases}$	O89
21	$He + \gamma \longmapsto He^+ + e^-$	$\sigma_{21} = 7.42\times10^{-18}\left[1.66\left(\frac{\nu}{\nu_\mathrm{th}}\right)^{-2.05} - 0.66\left(\frac{\nu}{\nu_\mathrm{th}}\right)^{-3.05}\right], \quad \nu > \nu_\mathrm{th}$	O89
22	$He^+ + \gamma \longmapsto He^{++} + e^-$	$\sigma_{22} = (A_0/Z^2)\left(\frac{\nu}{\nu_\mathrm{th}}\right)^{-4}\left[\frac{e^{(4-4\arctan\epsilon/\epsilon)}}{(1-e^{-2\pi/\epsilon})}\right]$, $h\nu_\mathrm{th} = Z^2\times13.6\,\mathrm{eV}$ and $Z = 2$.	O89
23	$H^- + \gamma \longmapsto H + e^-$	$\sigma_{23} = 7.928\times10^5(\nu-\nu_\mathrm{th})^{3/2}\left(\frac{1}{\nu^3}\right), \quad h\nu > h\nu_\mathrm{th} = 0.755\,\mathrm{eV}$	DeJ72
24	$H_2 + \gamma \longmapsto H_2^+ + e^-$	$\sigma_{24} = \begin{cases} 0 & : \quad h\nu < 15.42\,\mathrm{eV} \\ 6.2\times10^{-18}h\nu - 9.40\times10^{-17} & : \quad 15.42 < h\nu < 16.50\,\mathrm{eV} \\ 1.4\times10^{-18}h\nu - 1.48\times10^{-17} & : \quad 16.5 < h\nu < 17.7\,\mathrm{eV} \\ 2.5\times10^{-14}(h\nu)^{-2.71} & : \quad h\nu > 17.7\,\mathrm{eV} \end{cases}$	OR78
25	$H_2^+ + \gamma \longmapsto H + H^+$	$\sigma_{25} = 7.401\times10^{-18}10^{(-x^2-.0302x^3-.0158x^4)}$ $\begin{cases} x = 2.762\ln(h\nu/11.05\,\mathrm{eV}) \\ h\nu > 2.65\,\mathrm{eV} \end{cases}$	TSR97
26	$H_2^+ + \gamma \longmapsto 2H^+ + e^-$	$\sigma_{26} = 10^{-16.926-4.528\times10^{-2}h\nu+2.238\times10^{-4}(h\nu)^2+4.245\times10^{-7}(h\nu)^3}$, $30 < h\nu < 90\,\mathrm{eV}$	AAZN97
27	$H_2 + \gamma \longmapsto H_2^* \longmapsto H + H$	$\sigma_{27} = 3.71\times10^{-18}$, $12.24 < h\nu < 13.51\,\mathrm{eV}$	HRL96
28	$H_2 + \gamma \longmapsto H + H$	See reference for the expression	AAZN97

respectively, and we have assumed a monatomic energy budget of $\frac{3}{2}kT$ per particle (the energy associated with rotational and vibrational states of H_2 is negligible).

$$\Lambda_{\rm cool} = \Lambda_{\rm H,ce} + \Lambda_{\rm H,ci} + \Lambda_{\rm He^+,ce} + \Lambda_{\rm H_2,ce} + \Lambda_{\rm Compton} \quad (2)$$

where the suffixes 'ce' and 'ci' mean collisional excitation and ionization, respectively, and expressions for each of these terms are given in HSTC02.

$$\Lambda_{\rm heat} = \Lambda_{\rm H,pi} + \Lambda_{\rm He,pi} + \Lambda_{\rm He^+,pi} + \Lambda_{\rm H_2,pi} + \Lambda_{\rm H_2,pd}, \quad (3)$$

where the suffixes 'pi' and 'pd' mean heating from photoionization and photodissociation, respectively. The expression for each term was calculated using equation (B1) from the Appendix B, using the cross-sections listed in Table 1.

2.2 UV background spectrum

The non-equilibrium chemistry and the thermal evolution of the clouds are calculated assuming the presence of a UV radiation field of the power-law form

$$J_\nu = J_{21} \times \left(\frac{\nu}{\nu_{\rm H}}\right)^{-\alpha} 10^{-21}\,{\rm erg\,s^{-1}\,cm^{-2}\,Hz^{-1}\,sr^{-1}}, \quad (4)$$

where $h\nu_{\rm H} = 13.6\,{\rm eV}$ is the Lyman limit of H. Here, the direction of the radiation field is not important and the normalization is given in terms of the equivalent isotropic field.

In the present-day Universe, quasi-stellar objects (QSOs) have much steeper spectra ($\alpha \approx 1.8$, e.g. Zheng et al. 1997) than do stars ($\alpha \approx 5$, e.g. Barkana & Loeb 1999). However, Population III stars are likely to be biased to much higher spectral energies and their spectra may resemble those of QSOs above the Lyman limit (Tumlinson & Shull 2000; Tumlinson, Shull & Venkatesan 2003). In this paper, we take $\alpha = 2$ which could equally well apply to either type of source.

For the calculation of all the photoionization and photodissociation rates and as well as the heating terms, we assume an optical thin medium and no self-shielding.

2.3 Cooling of isolated clouds

Apart from a scaling factor, the cooling time, $t_{\rm cool}$, of isolated haloes subject to a uniform radiation field depends solely on the ratio of the number densities of baryons, $n_{\rm b}$, and photons, n_γ, that is, $t_{\rm cool} = {\rm fn}(T_{\rm vir}, n_{\rm b}/n_\gamma)/n_{\rm b}$. Thus, the effect of the global background radiation on single haloes can be presented in two ways: we can fix either the baryon density or the amplitude of the radiation field and vary the other.

Fig. 1 shows the cooling time, $t_{\rm cool}$, of haloes exposed to different levels of background radiation for a fixed density of $n_{\rm H} \approx 0.31\,{\rm cm^{-3}}$, corresponding to the mean density within a collapsed halo at $z = 20$, as seen from the J_{21}–$T_{\rm vir}$ plane. $t_{\rm cool}$ is defined as the time that the halo takes to cool from virialization to the moment when $T = 0.75T_{\rm vir}$ (or, if it does not cool, we stop the integration when the scalefactor reaches 10). Any halo that falls on the white region will not be able to cool in a Hubble time. On the other hand, haloes on the dark part of the plot will cool in much less than a dynamical time.

In Fig. 2, we show the fractional density of molecular hydrogen, $f_{\rm H_2}$, after one cooling time in the J_{21}–$T_{\rm vir}$ plane. The region that has not cooled by the time the scalefactor reaches 10 has been coloured white. For the zero-flux case, we see that the highest molecular fractions occur for a virial temperature of just over 10^4 K. Haloes of this temperature are able to partially ionize hydrogen atoms and the free electrons then go on to catalyze production of H_2.

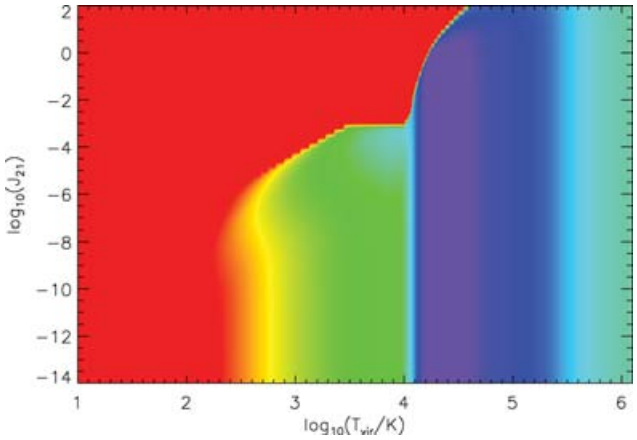

Figure 1. The cooling time, $t_{\rm cool}$ in the J_{21}–$T_{\rm vir}$ plane. The colour bar is $\log_{10}(t_{\rm cool}/{\rm yr})$. This plot was calculated at a fixed density corresponding to $z = 20$. Note that this figure and Fig. 2 look much nicer in colour in the on-line version of this paper.

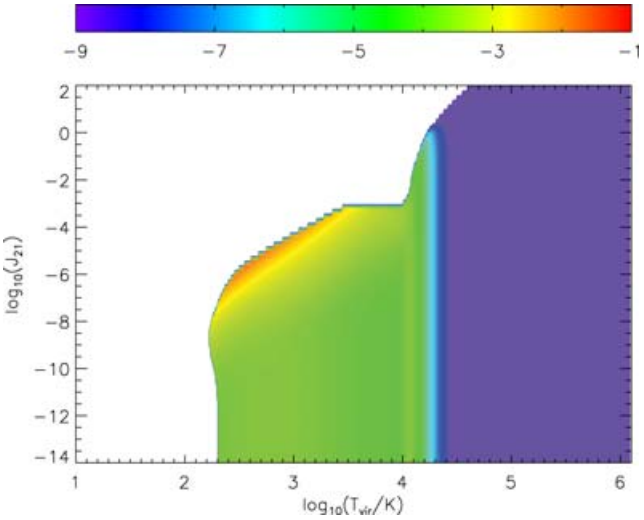

Figure 2. The molecular hydrogen fraction, $f_{\rm H_2}$, after one cooling time, in the J_{21}–T_{vir} plane. The region corresponding to clouds that have not cooled by the time the expansion factor reaches 10 has been coloured white.

From these plots, we can see that the ionizing radiation has two main effects. First, it provides a heat source that prevents cooling of haloes. The minimum virial temperature of haloes that can cool gradually increases along with the photon flux, whereas the heating has little effect on haloes above this temperature. The effect is visible in Fig. 1 as a sharp transition between the grey and white regions that runs diagonally across the plot.

Secondly, the ionizing flux can boost cooling of low-temperature haloes ($T_{\rm vir} \leqslant 10^4$ K) by creating free electrons that then catalyze the production of H_2. For any given temperature, there is only a narrow range of photon fluxes for which this is important before photoheating swamps the increased H_2 cooling.

Thus, as the background ionizing radiation builds up in the Universe, we expect there at first to be a small boost in the formation of low-temperature (low-mass) star clusters and then a sharp decline. The precise values of J_{21} at which this occurs will depend upon the redshift of structure formation [recall that the above plots are for a redshift of 20 and the required values of J_{21} will scale as $(1+z)^3$].

In Section 4, we consider both specific values of $J_{21} = 10^{-10}$, 10^{-5}, 10^{-2} and 10 and also a time-evolving ionization field.

3 MERGER TREE

In a previous paper, ST03, we generated merger histories of dark matter haloes using the Block Model of Cole & Kaiser (1988). In this model, a parent block of mass M_0 and density fluctuation δ_0 is halved producing two daughter blocks of mass $M_1 = M_0/2$. Extra power, drawn at random from a Gaussian distribution, is then added to one block and subtracted from the other in order to conserve the overall level of fluctuations in the root block. This process is then repeated until the desired resolution has been reached. The reader should note that the tree is produced by stepping back in time. Therefore, the formation of the daughter blocks occurs at a higher redshift than their parent block. A valid criticism of this model is that the mass distribution is not smooth, as each level changes in mass by a factor of 2. This discretization of mass is an undesirable constraint on our model and for this reason we have moved to a more realistic method of generating the merger tree.

We now use a Monte Carlo algorithm to generate the merger tree. There are a number of codes which use this technique (e.g. Kauffmann & White 1993; Somerville & Kolatt 1999); however, we have chosen the method proposed by Cole et al. (2000). In short, the code uses the extended Press–Schecter formalism to generate the merger histories of dark matter haloes, but we refer the reader to this paper for a complete discussion of the code. The main advantage of this method over the Block Model is that the discretization of mass has been removed.

Unlike most previous tree implementations, we do not place our merger tree on to a predefined grid of time-steps, but utilize a very fine time-resolution. This allows us to retain the Block Model's prescription of two progenitors per merger, consistent with our previous work. The algorithm allows us to account for the accretion of mass below the resolution limit; however, we assume that this will not seriously affect the structure and cooling of the halo.

An important aspect of the code is how we treat the mergers of haloes. The outcome of a merger will depend upon the ratio of masses of the merging haloes,

$$q = \frac{M_1}{M_2}, \tag{5}$$

where $M_1 < M_2$. Consequently, we introduce, $q_{\rm min}$, as the minimum mass ratio to affect the cooling of a halo. This leads to the following two cases.

(i) If $q > q_{\rm min}$, then the two haloes merge and their cooling is completely disrupted. The gas is then shock heated to the virial temperature of the parent halo, erasing all previous cooling information, and the cooling starts afresh.

(ii) If $q < q_{\rm min}$, then we assume that the smaller of the two daughters is disrupted. We then compare the times at which the larger daughter and the parent halo would cool. If the former occurs first then we postpone the merger and allow the cooling of the daughter to proceed; otherwise, we continue as for $q > q_{\rm min}$.

In the future we would like to determine an appropriate value for $q_{\rm min}$ from hydrodynamical simulations. Simulations of galaxy mergers (e.g. Mihos & Hernquist 1996) show that when objects with mass ratios $q > 0$ collide, the galactic structure of both objects is seriously disrupted. They classify these as 'major' mergers. We suspect that smaller mass ratios would still sufficiently disrupt the cooling gas cloud. Consequently, for this work we set $q_{\rm min} = 0.25$. Although we do not show it here, our results remain largely unchanged in the range $0.2 < q_{\rm min} < 0.3$.

We treat the metal enrichment of haloes in the same way as ST03 where it was assumed that, regardless of whether or not star clusters survive a merger, they instantly contaminate their surroundings with metals and the enrichment is confined to the next level of the merger hierarchy (i.e. the metals do not propagate into haloes on other branches). This is the same for both the global (Section 4) and local models (Section 5).

Once a halo has been contaminated it is no longer classed as primordial, irrespective of whether it can form more stars or not. However, no attempt is made to account for the transition from Population III to Population II star formation. Consequently, contaminated haloes are assumed to cool at the same rate as their primordial counterparts and in the case of our local model, produce the same ionizing flux. We intend to investigate the effect of this transition in future work by including cooling from metals.

In this paper, in common with ST03, we use a root mass of $10^{11}\,{\rm M}_\odot$ for our tree, and a mass resolution of $9.5 \times 10^4\,{\rm M}_\odot$. However, we use slightly different cosmological parameters as derived from the *Wilkinson Microwave Anisotropy Probe* (*WMAP*) data (Spergel et al. 2003) of $\Omega_0 = 0.3$, $\lambda_0 = 0.7$, $\Omega_{\rm b0} = 0.0457$, $h = 0.71$, $\sigma_8 = 0.9$, and a power spectrum as calculated by CMBFAST.

Fig. 3 shows a comparison between the new merger tree (solid line) and the older Block Model from ST03 (dashed line) of the fractional mass per dex of primordial star clusters as a function of virial temperature, averaged over a large number of realizations and in the absence of ionizing radiation. It is clear that the new tree has had a significant effect on the number of primordial objects that are formed. While the total number of objects that are able to cool remains roughly constant, our new model produces only a third of the primordial objects compared with the original, although the mass fraction has only been reduced by half. Qualitatively, the results remain unchanged: we still observe two generations of haloes, distinguished by their primary cooling mechanism, as discussed in ST03. In addition, we have removed all features associated with the discrete mass steps (e.g. the feature at ∼5000 K in the original model).

The smoothed mass distribution has led to many unequal-mass mergers which were not present in the previous model, thus, increasing the likelihood of contaminating large haloes with much smaller ones which happen to cool first. Equally, the chance that

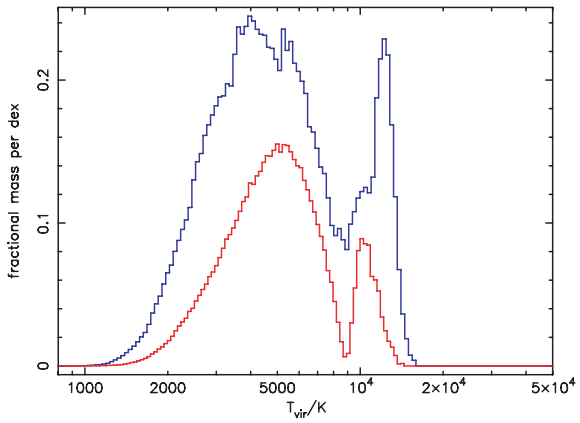

Figure 3. The fractional mass per dex of primordial star clusters as a function of virial temperature: solid line – new merger tree, dashed line – Block Model.

haloes are involved in mergers that disrupt their cooling is increased. These effects conspire to reduce the overall number of primordial objects.

4 GLOBAL IONIZATION FIELD

4.1 Model

In this section, we consider the effect of a global ionization field that affects all haloes equally. As previously mentioned, we will restrict ourselves to a power-law ionizing flux with index $\alpha = 2$, corresponding either to a quasar spectrum or that of stars of primordial composition. We present results for four cases of constant normalization: $J_{21} = 10^{-10}$, 10^{-5}, 10^{-2} and 10. These are chosen to be representative of a very low flux where the effect on each halo is minimal; a flux which has a positive effect on the capacity of the gas to form H_2; and two examples of higher-amplitude fluxes that destroy H_2.

In addition to the cases outlined above, we consider a time-dependent build-up of the background flux. Using radiative hydrodynamical calculations to examine the effect of the UV background on the collapse of pre-galactic clouds, Kitayama et al. (2000) modelled the evolution of a UV background as

$$J_{21}(z) = \begin{cases} \mathrm{e}^{-\beta(z-5)} & : \quad 5 \leqslant z \leqslant z_{\rm uv} \\ 1 & : \quad 3 \leqslant z \leqslant 5 \\ (\frac{1+z}{4})^4 & : \quad 0 \leqslant z \leqslant 3. \end{cases}$$

We adopt their model and fiducially fix the onset of the UV background at $z_{\rm uv} = 50$ (at which time the normalization is negligible). We have added a factor of β into this expression so as to control the rate at which the field builds up and present results for three cases: $\beta = 0.8$ (rapid), 1 (standard), and 2 (slow).

For the latter cases especially, the global ionizing flux can be thought of as coming from pre-existing star clusters (or quasars) that form in high-density regions of space and that are gradually ionizing the Universe around them. For this reason, we take the mean density of the tree to be equal to that of the background Universe. In Section 5, we will consider a high-density region for which the ionization field is generated internally from the star clusters that form in the tree.

4.2 Results

In Fig. 4, we plot the fractional mass of primordial star clusters as a function of (a) virial temperature and (b) halo mass. The dash–dotted, dashed, dotted, and solid lines correspond to $J_{21} = 10^{-10}$, 10^{-5}, 10^{-2} and 10, respectively – note that, the peak of the distributions does *not* move steadily from the left-hand to right-hand side as J_{21} is increased. Fig. 5 shows histograms of the star formation redshifts of the primordial clusters.

The lowest amplitude case is almost indistinguishable from that of zero flux. For this reason, we have not plotted the latter. There are two bumps in the virial temperature histogram corresponding to two distinct cooling mechanisms. In ST03, these were christened Generation 1 (low virial temperature, $T \leqslant 8600$ K, low-mass, high-collapse redshift, dominated by H_2 cooling) and Generation 2 (high virial temperature, $T \geqslant 8600$ K, high-mass, low-collapse redshift, dominated by electronic cooling).

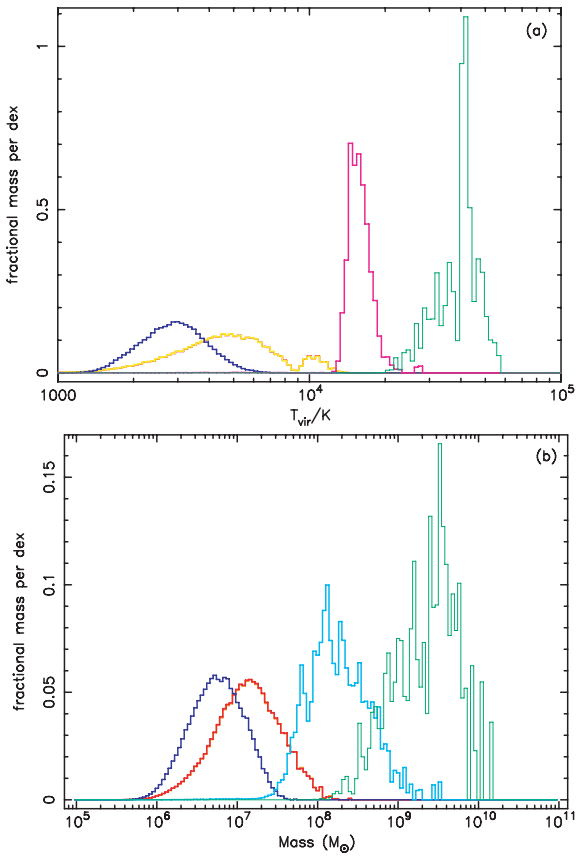

Figure 4. Fractional mass per dex of primordial objects as a function of (a) virial temperature and (b) mass, for four different cases: the dash–dotted line corresponds to $J_{21} = 10^{-10}$; the dashed line to $J_{21} = 10^{-5}$; the dotted line to $J_{21} = 10^{-2}$; and the solid line to $J_{21} = 10$.

As the flux is increased, the effect of the radiation field is to promote the cooling of Generation 1 haloes. The typical virial temperature and mass of such haloes decrease, and the number of Generation 2 star clusters is reduced as collapsing haloes are more likely to have been polluted by metals from smaller objects within them. For $J_{21} = 10^{-5}$ (dashed curve), the effect is so pronounced that it completely eliminates Generation 2 objects. However, this is an extreme case, because, as Figs 1 and 2 show, this flux has been chosen to produce close to the maximum possible enhancement in the H_2 fraction and a corresponding reduction in cooling time throughout the redshifts at which these haloes form.

If the background flux is increased further, then the enhancement in Generation 1 star clusters is reversed. For $J_{21} = 10^{-2}$ (dotted curve), the balance has shifted almost entirely in the favour of Generation 2 clusters and by $J_{21} = 10$ all Generation 1 clusters have been eradicated.

It is interesting to note that the mass fraction of stars contained in primordial star clusters is not greatly affected by the normalization of the ionizing radiation, varying from 0.05 to 0.1. However, the mass (and hence number) of the star clusters varies substantially. A modest flux will increase the number of small clusters, moving the mass function to lower masses, while a greater flux produces the opposite effect.

The number of primordial star clusters as a function of star formation redshift is shown in Fig. 5. The redshift distribution is similar in all cases, which differs significantly from model with time-varying flux, discussed next.

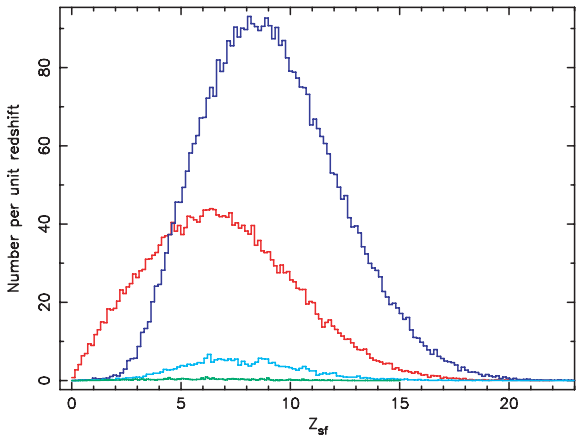

Figure 5. Histograms of star formation redshifts for primordial haloes. The line-style coding is the same as in Fig. 4.

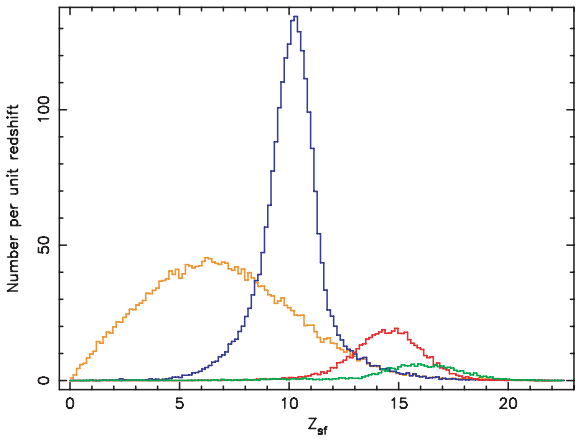

Figure 7. Histograms of star formation redshifts for primordial haloes. The line-style coding is the same as in Fig. 6.

Fig. 6 plots the fractional mass of primordial star clusters, as a function of (a) virial temperature and (b) mass. Unlike our previous results, the introduction of a time-evolving field has had a devastating effect on the mass fraction of primordial objects. As the rate at which the flux builds-up increases, the peak of the Generation 1 mass function moves towards lower masses (and virial temperatures) and its normalization decreases significantly. At the same time, as shown in Fig. 7, the peak in the production rate moves to higher redhsifts. In each case, it corresponds to a flux of $J_{21} \approx 5 \times 10^{-5}$ for which, from the previous results, an enhancement in the H_2 fraction and, hence, a decrease in the cooling time is expected.

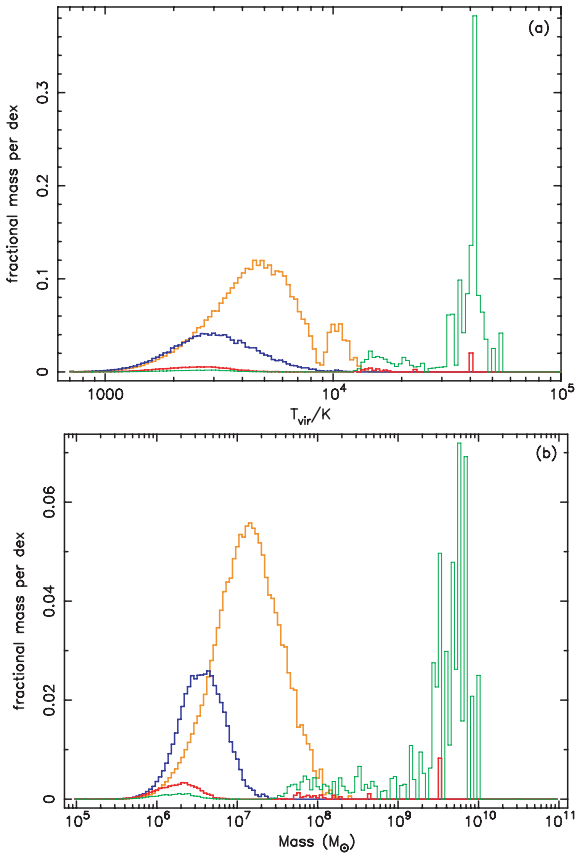

Figure 6. Fractional mass per dex of primordial objects as a function of (a) virial temperature and (b) mass, for four different cases: the dash–dotted line corresponds to the no-flux case; the dashed line to $\beta = 2$; the dotted line to $\beta = 1$; and the solid line to $\beta = 0.8$.

The effect on the production of higher-mass, higher virial temperature star clusters, is more complicated. In this paper, we are concerned with primordial objects, by which we mean those with zero metallicity. The key question, then, is whether large haloes are contaminated by metals from subclusters within them. With a slow build-up of flux, cooling in these subclusters is enhanced, resulting in increased contamination and a reduction in the number density of primordial Generation 2 haloes. However, a rapid build-up of flux cuts off production of small haloes dramatically, and the number of primordial Generation 2 haloes is increased.

5 LOCAL FEEDBACK

In this section, we consider local feedback, that is, that produced by star clusters internal to the tree.

5.1 Model

5.1.1 Physical picture and assumptions

The large value of the Thomson electron-scattering optical depth in the *WMAP* data of $\tau = 0.17 \pm 0.04$ (Spergel et al. 2003) suggests an early re-ionization era at $11 < z < 30$ (180^{+220}_{-80} Myr after the big bang). This requires a high efficiency of ionizing photon production in the first stars, corresponding to a deficit of low-mass stars. This is backed up by theoretical arguments and simulations (e.g. Abel, Bryan & Norman 2002; Bromm, Coppi & Larson 2002; Schaerer 2002; Tumlinson, Venkatesan & Shull 2004; Santoro & Shull 2005) of star formation in a primordial gas, for which fragmentation was found to be strongly inhibited by inefficient cooling at metallicities below about $10^{-3.5}\,Z_\odot$.

There is still some debate as to whether the first star-forming haloes will produce a single massive star (e.g. Abel et al. 2002) or fragment further to form the first star clusters (e.g. Bromm et al. 1999). Whichever of these is correct makes little difference to our results. Tumlinson et al. (2004) considered a number of IMFs that may lead to the required early re-ionization. These have ionizing fluxes per unit mass in the range $Q \approx 10^{47}$–10^{48} ph s^{-1} $M_\odot^{-1}$, but they all have similar ionizing efficiencies of about 80 000 photons/baryon

Table 2. Parameters of the ionization models that we consider: model number; fraction of mass in stars, f_*; specific ionizing fluxes, Q_0, in units of ph s^{-1} M$_\odot^{-1}$; total number of ionizing photons, N_0, and ionizing flux, S_0, in units of ph s^{-1} M$_\odot^{-1}$ of matter (baryonic plus dark); and the time for which the ionizing flux acts, t_*, in units of years.

Id	f_*	Q_0	N_0	S_0	t_*
1 (solid)	10^{-2}	10^{48}	1.5×10^{59}	1.5×10^{45}	3×10^6
2 (dashed)	10^{-3}	10^{48}	1.5×10^{58}	1.5×10^{44}	3×10^6
3 (dotted)	10^{-3}	10^{47}	1.5×10^{58}	1.5×10^{43}	3×10^7

when integrated over the whole life of the stars, a value which is similar to that obtained for single massive stars ($M \gtrsim 20\,\mathrm{M}_\odot$). If we assume a uniform flux over time, then this corresponds to mean lifetimes of 3.0×10^7–3.0×10^6 yr, respectively. Note that these values of Q are much greater than the average for the Milky Way, $Q \approx 8.75 \times 10^{43}$ ph s^{-1} M$_\odot^{-1}$ (Ricotti & Shull 2000).

When haloes in the merger tree are able to cool, we assume that they will convert part of their baryonic component into a 'star cluster' (primordial or otherwise). These objects will exert radiative feedback on to the next generation of haloes that form inside the same tree. The photon flux will also depend upon the star formation efficiency and the escape fraction from the star-forming region in the centre of the halo. In this paper, we are not concerned with the magnitude of metal production and so it is only the combination of the two, f_*, that is of interest.

The total ionizing flux from a halo is

$$S = f_* M_\mathrm{b} Q, \tag{6}$$

where $M_\mathrm{b} \approx 0.152\,M$ is the baryonic mass and M is the total mass of the halo. We will present results for three models, listed in Table 2. Model 1 has the highest ionizing flux; model 2 has a smaller flux but lasts for the same length of time; model 3 has an even smaller flux but lasts for longer so that the total number of ionizing photons produced is the same as for model 2.

Once the stars have formed, the ionizing photons will begin to evaporate the rest of the halo and make their way into the surrounding IGM. Each star cluster produces

$$N_\gamma = 80\,000\,\frac{f_* M_\mathrm{b}}{m_\mathrm{H}} \tag{7}$$

ionizing photons, where M_b is the baryonic mass. In the absence of recombination, this is sufficient to ionize the hydrogen in a region of baryonic mass

$$M_{\mathrm{b}\gamma} = N_\gamma\,\mu_\mathrm{H} m_\mathrm{H}, \tag{8}$$

where $\mu_\mathrm{H} \approx 1.36$ is the mean molecular mass per hydrogen nucleus. For the star formation efficiencies and top-heavy IMF that we consider here, there are more than enough photons to ionize any neutral gas within the star cluster:

$$\frac{M_{\mathrm{b}\gamma}}{M_\mathrm{b}} = 80\,000\,f_*\,\mu_\mathrm{H} \approx 1.1 \times 10^5\,f_*. \tag{9}$$

We next consider whether it is correct to neglect recombinations. The photon flux required to maintain ionization of the halo (at the mean halo density) is given by

$$S_\mathrm{halo} = \frac{4\pi}{3}\,R^3\,n_\mathrm{H}^2\,\mathcal{R}, \tag{10}$$

where R is the radius of the virialized halo, n_H is the combined number density of all species of hydrogen, and $\mathcal{R}$ is the recombination rate (see, e.g. HSTC02). The value of S_halo would be higher if we were to take into account clumping of the gas. On the other hand, there are two effects that will tend to lower S_halo: for high-temperature haloes not all the gas will be neutral; for low-temperature haloes the gas will be raised to a temperature that exceeds the virial temperature and so will tend to escape from the halo – the sound-crossing time for a gas at 10^4 K is of the order of 1.0×10^7 yr for a 10^6-M$_\odot$ halo at an expansion factor $a = 0.05$. We assume that these effects will roughly cancel and set the nett photon flux that escapes the halo equal to $S_\mathrm{esc} = S - S_\mathrm{halo} = f_\mathrm{esc}\,S$. Here

$$1 - f_\mathrm{esc} = \frac{S_\mathrm{halo}}{S} \approx 0.12\left(\frac{a}{0.05}\right)^{-3}\left(\frac{S_0}{1.5 \times 10^{44}\,\mathrm{ph\,s^{-1}}}\right)^{-1}, \tag{11}$$

where we have set $\mathcal{R}$ equal to the recombination rate for a 10^4-K gas. Of course, f_esc is not allowed to drop below zero. The number of ionizing photons that escape the source halo is

$$N_{\mathrm{b}\gamma,\mathrm{esc}} = f_\mathrm{esc} N_{\mathrm{b}\gamma}. \tag{12}$$

Escaping photons are now free to propagate into the inter halo medium (aka IGM) and irradiate nearby haloes. At the mean density of the IGM, the Strömgren radii for any ionized regions are very large, and only model 1 produces enough photons to ionize out to the Strömgren radius, and then only at very early times, $a \lesssim 0.02$. A better picture is that of a bubble of ionized gas whose outer radius grows with time until the ionizing source switches off. To a good approximation then, and for simplicity, we assume that recombinations in the IGM are negligible.

5.1.2 Numerical methodology

The local feedback is implemented as follows. First, the tree is scanned for all star clusters and a list is generated, in order of decreasing star formation redshift. Starting with the first cluster, we work up the tree looking at the baryonic mass of successive parent haloes, $M_\mathrm{b,par}$, until the last halo for which

$$M_\mathrm{b,par} < M_\mathrm{b} + M_{\mathrm{b}\gamma,\mathrm{esc}}. \tag{13}$$

The subtree below this parent halo (see Fig. 8) defines the extent of the ionized region, and the cooling times of all haloes within it are recalculated taking into account the amplitude of the flux and the time for which it acts.

The tree provides limited information about the spatial distribution of haloes. However, we know that haloes are confined within a common parent halo, and that the parent will not have collapsed at this time. So we take the separation of the star cluster and each neighbouring halo to be equal to the radius of a sphere at the mean density at that time that encloses a mass equal to that of the first common parent:

$$R_\mathrm{par} = a\left(\frac{3M_\mathrm{b,par}}{4\,\pi\,\Omega_{\mathrm{b}0}\,\rho_{\mathrm{c}0}}\right)^{1/3}, \tag{14}$$

where a is the scalefactor at the time of star formation and the other quantities have the usual meanings. Note that the value of $M_\mathrm{b,par}$ in equation (14) will vary depending upon how far one has to travel up the tree to find a common neighbour.

The flux density, F, at a distance R_par from the source is given by

$$F = \frac{S_\mathrm{esc}}{4\pi R_\mathrm{par}^2}. \tag{15}$$

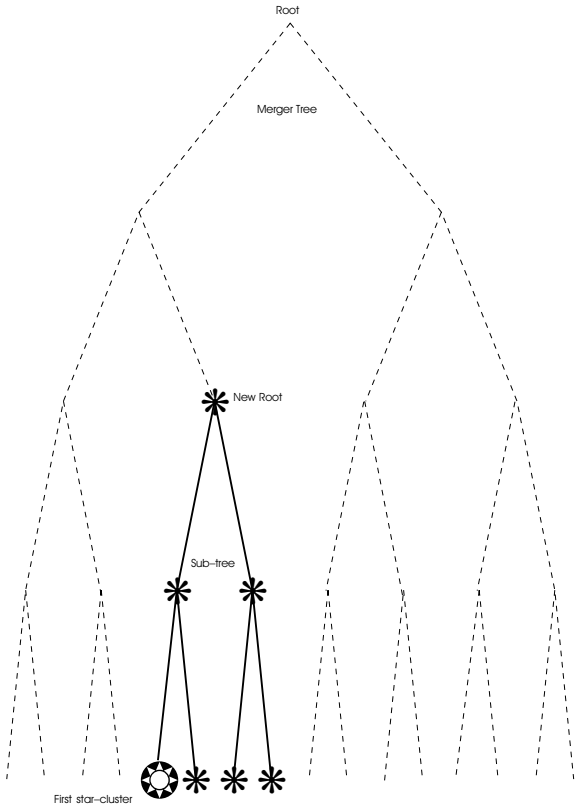

Figure 8. Schematic view of the merger tree under internal feedback. Once the first star cluster is located, the code calculates how many levels up the tree has to go to re-calculate the cooling times of each halo under the new root, this time under the influence of the radiative flux coming from that first star cluster. In this example, the feedback region reaches two levels up the tree. Then, the whole subtree cooling times will be re-evaluated.

We need to convert this into an equivalent value of J_{21} for input into our chemical evolution code. To do this we integrate the spectrum given in equation (4) over all frequencies and angles:

$$F = 4\pi \int_{\nu_{\rm H}}^{\infty} \frac{J_\nu}{h\nu}\, {\rm d}\nu = \frac{4\pi}{\alpha} J_{21}, \qquad (16)$$

where $h\nu_{\rm H} = 13.6\,{\rm eV}$ is the energy of H ionization. Combining these two equations allows us to express the ionizing flux as an equivalent value of J_{21} for an isotropic radiation field (the directionality of the radiation field is unimportant in this context). We use the value of J_{21} and duration of the ionization as inputs to the chemistry code to obtain the new cooling time of each neighbouring halo in the subtree, using the heating and cooling processes explained in Section 2.3.

The list of remaining clusters is then re-ordered using the new star formation redshifts and we continue with the next halo in the list. The process is repeated until we reach the bottom of the list or until the next halo in the list is not able to cool in a Hubble time.

5.2 Results

The first stars are widely predicted to form in high-density regions of space. Consequently, in this section, we present results of simulations with internal radiative feedback in a region for which the root halo corresponds to a positive 3σ density fluctuation.

Fig. 9 plots histograms of star formation redshifts for primordial haloes for the three cases shown in Table 2, averaged over a large number of realizations. It is evident that the redshift evolution is markedly different for the three curves and we will discuss each in turn.

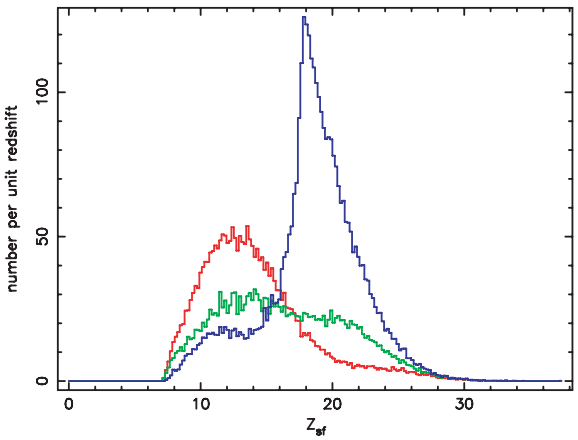

Figure 9. Histograms of the star formation redshifts of primordial star clusters, averaged over a large number of realizations. The line styles correspond to different models of local feedback as listed in Table 2.

First of all, in Fig. 10, we compare model 3 with the case of zero flux. We can clearly see that the evolution of the two curves is identical up to a point, after which model 3 drops away dramatically. This sudden change can be understood by examining equation (11). We are interested in the redshift at which the ionizing photons first begin to escape the halo. If we set $f_{\rm esc}$ equal to zero and solve for the scalefactor, a, we find that, for this particular model, photons do not break out until a redshift $z \sim 18$, in agreement with what is seen in Fig. 10. Also shown are the contributions from the two different halo generations, discussed in previous sections. The escaping photons have had a devastating impact on the surrounding haloes, particularly the smaller, Generation 1 haloes. As a result there is a rise in the number of Generation 2 haloes, because the reduced contamination at early times allows more massive haloes to cool as primordial objects.

In models 1 and 2, the photons are able to escape the halo at much earlier times (before any objects have been able to cool). As such, the first primordial objects to form will immediately begin to influence their surroundings. This explains the much greater reduction

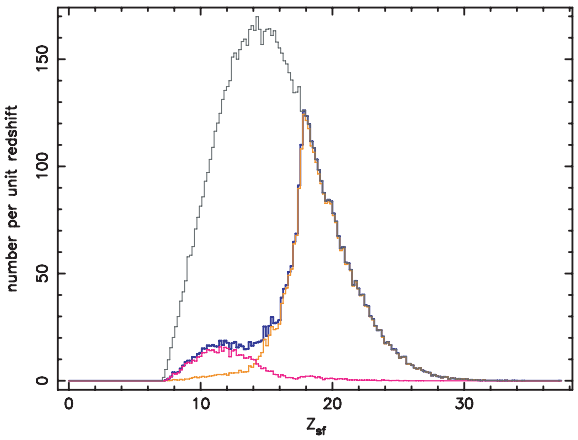

Figure 10. Histogram of star formation redshifts for primordial haloes. Here, we compare model 3 (the thick solid line) with the no-flux case (the thin solid line). Also shown are the contributions from the Generation 1 (the dashed line) and Generation 2 (the dotted line) haloes.

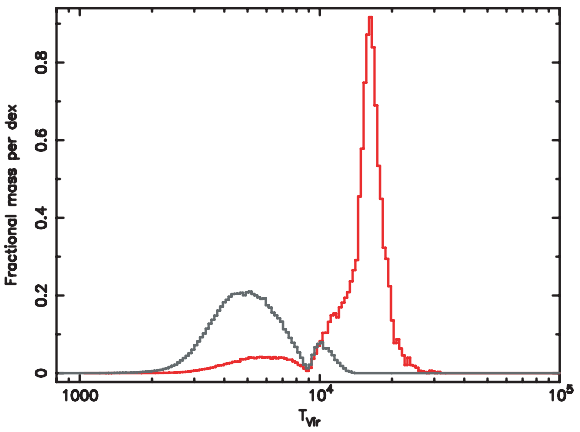

Figure 11. Fractional mass per dex of primordial objects as a function of temperature, for model 1 (the thick line) and the no-flux case (the thin line).

in Generation 1 star clusters for these models compared to model 3, seen in Fig. 9.

Fig. 11 plots the fractional mass per dex of primordial objects as a function of temperature for our highest-flux case (model 1). As expected, the higher flux has suppressed the small, low-temperature haloes at high redshift, thus, reducing the amount of early contamination. Once again we see that there has been an enhancement in the number of high-temperature, high-mass haloes, the distribution of which is reminiscent of that seen in Fig. 4 for the high values of J_{21} in our global model, particularly $J_{21} = 10^{-2}$. Indeed, the average J_{21} values received by haloes in this model are in the range $J_{21} = 10^{-3}$–10^{-2}, consistent with our previous results.

With 10 times fewer photons, we expect model 2 to be less destructive than model 1 at higher redshifts and Fig. 9 confirms this fact. The dashed curve shows more primordial objects early on which consequently reduces the number of Generation 2 objects that form. Interestingly, this model shows an approximate balance between the two generations with a roughly constant formation rate of primordial haloes between the redshifts $z \sim 10$ and 22.

The mass fraction of stars contained in primordial star clusters for all the models presented here remains relatively constant, varying from 0.06 to 0.13. However, the mass functions vary substantially as do the star formation histories. As the specific ionizing flux increases, the balance moves towards later star formation and more Generation 2 primordial star clusters. The positive feedback into Generation 1 clusters seen in Fig. 4 for intermediate values of J_{21} lasts for too short a time to be noticeable.

6 DISCUSSION

This paper looks at the impact of radiative feedback on primordial structure formation. This is done in two ways.

The first part investigates the properties of primordial objects under a global UV background. The merger tree is illuminated by a constant and isotropic radiation field of four different intensities, parametrized by a constant value of J_{21} : 10^{-10}, 10^{-5}, 10^{-2} and 10. It seems more plausible that any background radiation field would gradually build up over time with the formation of more and more primordial stars. Consequently, we also investigate a time-dependent build-up of the background flux using an extension of the model of Kitayama et al. (2000). This section of the paper uses a mean-density region of space, as the background radiation field is assumed to come from external sources within higher-density regions.

The effect of a constant UV field on the halo population is not a trivial one as both positive and negative feedback can arise from different choices of the flux amplitude J_{21}. The cooling of a low-temperature primordial gas is almost completely dominated by the release of energy from roto-vibrational line excitation of H_2. But if a radiation field is present, H_2 is easily destroyed by Lyman–Werner photons ($11.2 < h\nu < 13.6$ eV). On the other hand, the formation of H_2 can be enhanced by an increase in the ionization fraction produced by a weak ionizing flux, as electrons act as a catalyst for the formation path of H_2. At modest flux levels of $J_{21} \sim 10^{-5}$, the nett effect is to boost cooling in the first star clusters. A similar result has previously been found by Haiman et al. (1996), Ricotti, Gnedin & Shull (2001), Kitayama et al. (2001) and Yoshida et al. (2003).

Negative feedback is produced not only by photodissociation of H_2; at high flux levels the dominant effect comes from heating associated with photoionization of H. For fluxes of $J_{21} \geqslant 10^{-2}$, we find that molecular cooling is ineffective and only haloes with virial temperatures of $T_{\rm vir} > 14\,000$ K are able to cool in a Hubble time. Because of reduced contamination from star formation in low-mass haloes, strong radiation fields can increase the number of high-mass primordial star clusters.

The second part of this paper dealt with a model in which the radiative feedback is localized. That is, star clusters irradiate their surrounding area, changing the cooling properties of those primordial objects that are inside their ionization spheres. For this model we considered only a high-density region corresponding to a 3σ fluctuation, because the first objects are thought to form in regions of high overdensity.

The effect of the feedback depends mainly upon the specific ionizing flux, averaged over the mass of the halo. When this is low, most or all of the photons will be used up in maintaining the ionization of the halo. For the particular model that we described in this paper, equation (11) relates the escape fraction, $f_{\rm esc}$, of ionizing photons to the specific ionizing flux, S_0, and redshift. A value of S_0 below 10^{43} ph s^{-1} M$_\odot^{-1}$ will reduce $f_{\rm esc}$ to zero until the redshift drops to about 16, corresponding to the peak in the production rate of primordial haloes per unit redshift. Although the precise number will be model-dependent, we regard this as a fiducial value below which feedback will be ineffective.

Higher values of S_0 result in shift from primordial star clusters away from Generation 1 (low virial temperature) towards Generation 2 (high virial temperature). Unlike the case of a global ionization field, Generation 1 clusters are not erradicated completely, because some must form in order to provide the feedback. However, a specific ionization flux of $S_0 = 10^{45}$ ph s^{-1} M$_\odot^{-1}$ is enough to swing the balance strongly in favour of the Generation 2 star clusters.

This paper makes a number of advances on our previous modelling, most notably the use of an improved merger tree that does not restrict haloes to factors of 2 in mass, and the introduction of a radiation field. The former results in a reduced mass fraction of stars in primordial haloes with the bias shifting more in favour of Generation 1; however, the latter moves the bias back the other way. The conclusions of HSTC02 and ST03 remain valid in that there could be a substantial population of primordial star clusters that form in high-mass haloes dominated via electronic cooling.

Further improvements to our model are possible. Although we do not expect these to change our qualitative conclusions, they will be important for making precise quantitative predictions about the number density and composition of the first star clusters. We mention some of them below.

We assume in this paper that the internal structure of haloes is unaltered between major merger events. However, it is possible for haloes to increase their mass substantially through a succession of minor accretion events, and this will release gravitational potential energy and lead to heating (Yoshida et al. 2003; Reed et al. 2005). We intend to incorporate this in future work.

No attempt has been made to distinguish between star formation and feedback in primordial star clusters and later generations. It is expected that the IMF should alter considerably once the metallicity reaches about $10^{-3.5}\,Z_{\odot}$ (Schneider et al. 2002; Bromm & Loeb 2003; Santoro & Shull 2005) and that the spectrum of the ionization field would become softer and its normalization lower.

We have neglected the effect of stellar winds and supernovae, both of which help to heat the surrounding gas and pollute it with metals. The effect of winds is fairly localized, but supernovae can lead to superwinds that expel enriched material from the star cluster. It is possible that this could affect neighbouring haloes; more likely it will simply ensure thorough mixing of metals throughout a common parent halo. Numerical simulations will be required in order to model this process with any degree of realism.

Finally, it would be valuable as computing resources improve to simulate larger regions of space that would provide a more respresentative section of the Universe. This would allow us to distinguish between the early history of galaxies that are located within clusters and in mean density regions of space, for example. It would also allow for both localized feedback and a self-consistent build-up of the background, global radiation field.

ACKNOWLEDGMENTS

MAM is supported by a PPARC studentship.

REFERENCES

Abel T., Anninos P., Zhang Y., Norman M. L., 1997, New Astron., 2, 181
Abel T., Anninos P., Norman M. L., Zhang Y., 1998, ApJ, 508, 518
Abel T., Bryan G. L., Norman M. L., 2002, Sci, 295, 93
Barkana R., Loeb A., 1999, ApJ, 523, 54
Bromm V., Loeb A., 2003, Nat, 425, 812
Bromm V., Coppi P. S., Larson R. B., 1999, ApJ, 527, L5
Bromm V., Coppi P. S., Larson R. B., 2002, ApJ, 564, 23
Cen R., 2003, ApJ, 591, L5
Ciardi B., Ferrara A., White S., 2003, MNRAS, 344, L7
Cole S., Kaiser N., 1988, MNRAS, 233, 637
Cole S., Lacey C. G., Baugh C. M., Frenk C. S., 2000, MNRAS, 319, 168
de Jong T., 1972, A&A, 20, 263
Glover S. C. O., Brand P. W. J. L., 2001, MNRAS, 321, 385
Haiman Z., Abel T., Rees M. J., 2000, ApJ, 534, 11
Haiman Z., Rees M. J., Loeb A., 1996, ApJ, 467, 522
Hutchings R. M., Santoro F., Thomas P. A., Couchman H. M. P., 2002, MNRAS, 330, 927 (HSTC02)
Kauffmann G., White S. D. M., 1993, MNRAS, 261, 921
Kitayama T., Tajiri Y., Umemura M., Susa H., Ikeuchi S., 2000, MNRAS, 315, L1
Kitayama T., Susa H., Umemura M., Ikeuchi S., 2001, MNRAS, 326, 1353
Machacek M. E., Bryan G. L., Abel T., 2001, ApJ, 548, 509
Mihos J. C., Hernquist L., 1996, ApJ, 464, 641
Oh S. P., Haiman Z., 2002, ApJ, 569, 558
Omukai K., 2001, ApJ, 546, 635
O'Neil S. V., Reinhardt W., 1978, J. Chem. Phys., 69, 2126
Osterbrock D. E., 1989, Astrophysics of Gaseous Nebulae and Active Galactic Nuclei. University Science Books, Mill Valley
Reed D., Bower R., Frenk C. S., Gao L., Jenkins A., Theuns T., White S. D. M., 2005, MNRAS, 363, 393
Ricotti M., Shull J. M., 2000, ApJ, 542, 548
Ricotti M., Gnedin N. Y., Shull J. M., 2001, ApJ, 560, 580
Ricotti M., Gnedin N. Y., Shull J. M., 2002, ApJ, 575, 33
Santoro F., Shull J. M., 2005, ApJ, submitted (astro-ph/0509101)
Santoro F., Thomas P. A., 2003, MNRAS, 340, 1240 (ST03)
Schaerer D., 2002, A&A, 382, 28
Schneider R., Ferrara A., Natarajan P., Omukai K., 2002, ApJ, 571, 30
Somerville R. S., Kolatt T. S., 1999, MNRAS, 305, 1
Spergel D. N. et al., 2003, ApJS, 148, 175
Tegmark M., Silk J., Rees M. J., Blanchard A., Abel T., Palla F., 1997, ApJ, 474, 1
Tumlinson J., Shull J. M., 2000, ApJ, 528, L65
Tumlinson J., Shull J. M., Venkatesan A., 2003, ApJ, 584, 608
Tumlinson J., Venkatesan A., Shull J. M., 2004, ApJ, 612, 602
Yoshida N., Abel T., Hernquist L., Sugiyama N., 2003, ApJ, 592, 645
Zheng W., Kriss G. A., Telfer R. C., Grimes J. P., Davidsen A. F., 1997, ApJ, 475, 469

The appendix below describes how to go from cross-sections to reaction rates and heating terms.

APPENDIX A: PHOTOIONIZATION AND PHOTODISSOCIATION INTEGRALS

The rate at which photoionization or photodissociation reactions occur is given by

$$k_i = 4\pi \int_{\nu_{\rm th}}^{\infty} \sigma_{\nu,i}\, \frac{J_\nu}{h\nu}\, {\rm d}\nu, \tag{A1}$$

where $h\nu_{\rm th}$ is the threshold energy for which photoionization (or photodissociation) is possible and $\sigma_{\nu,i}$ is the frequency-dependent cross-section of the ith reaction. The cross-section and the threshold energies were taken from Table 1. J_ν is the specific intensity given in equation (4).

APPENDIX B: HEATING TERMS

The energy per particle that a photon of energy $h\nu$ transfered to an electron in an atom or ion is $h\nu - h\nu_{\rm th}$. Therefore, the energy per second per unit volume transferred to the gas (heating terms or heating functions) is

$$\Lambda_{{\rm heat},i} = 4\pi n_i \int_{\nu_{\rm th}}^{\infty} \sigma_{\nu,i}\, J_\nu\, \frac{(\nu - \nu_{\rm th})}{\nu}\, {\rm d}\nu, \tag{B1}$$

where n_i is the number density of the dissociated species.

The heating of a primordial gas comes primarily from photoionization of H, He and He^+, but there is also a small contribution from photodissociation of H_2.

This paper has been typeset from a TEX/LATEX file prepared by the author.